Structural Engineering and Mechanics, *Vol. 81, No. 3 (2022) 349-365*
https://doi.org/10.12989/sem.2022.81.3.349

Curvature-based analysis of concrete beams reinforced with steel bars and fibres

Gintaris Kaklauskas*[1], Aleksandr Sokolov[2a], Ashkan Shakeri[1b], Pui-Lam Ng[3,4c] and Joaquim A.O. Barros[5,6d]

[1]*Department of Reinforced Concrete Structures and Geotechnics, Vilnius Gediminas Technical University, Sauletekio av. 11, 10223 Vilnius, Lithuania*
[2]*Laboratory of Innovative Building Structures, Vilnius Gediminas Technical University, Sauletekio av. 11, 10223 Vilnius, Lithuania*
[3]*Institute of Building Materials, Vilnius Gediminas Technical University, Linkmenų g. 28, 08217 Vilnius, Lithuania*
[4]*Department of Civil Engineering, The University of Hong Kong, Pokfulan 999077 Hong Kong, China*
[5]*Institute for Sustainability and Innovation in Structural Engineering, University of Minho, Campus de Azurém 4800-058 Guimarães, Portugal*
[6]*Institute of Science and Innovation for Bio-Sustainability, University of Minho, Campus de Azurém 4804-533 Guimarães, Portugal*

(*Received April 29, 2020, Revised October 25, 2021, Accepted November 19, 2021*)

Abstract. Steel fibre-reinforced concrete (SFRC) is an emerging class of composite for construction. However, a reliable method to assess the flexural behaviour of SFRC structural member is in lack. An analytical technique is proposed for determining the moment-curvature response of concrete beams reinforced with steel fibres and longitudinal bars (R/SFRC members). The behaviour of the tensile zone of such members is highly complex due to the interaction between the residual (tension softening) stresses of SFRC and the tension stiffening stresses. The current study suggests a transparent and mechanically sound method to combine these two stress concepts. Tension stiffening is modelled by the reinforcement-related approach assuming that the corresponding stresses act in the area of tensile reinforcement. The effect is quantified based on the analogy between the R/SFRC member and the equivalent RC member having identical geometry and materials except fibres. It is assumed that the resultant tension stiffening force for the R/SFRC member can be calculated as for the equivalent RC member providing that the reinforcement strain in the cracked section of these members is the same. The resultant tension stiffening force can be defined from the moment-curvature relation of the equivalent RC member using an inverse technique. The residual stress is calculated using an existing model that eliminates the need for dedicated mechanical testing. The proposed analytical technique was validated against test data of R/SFRC beams and slabs.

Keywords: deformation; moment-curvature; steel fibre-reinforced concrete; tension stiffening

1. Introduction

Low tensile strength and brittleness are two main shortcomings of concrete as a structural material. Due to low tensile strength, concrete cracks and its post-cracking tensile capacity banishes abruptly with the crack opening due to the concrete fragility. One of the ways of increasing toughness and crack resistance of concrete is by adding steel fibres to its mix composition, resulting in a composite designated as steel fibre-–reinforced concrete (SFRC) when fibres are made of steel. This significantly increases the post-cracking tensile capacity and energy absorption capability of cement-based materials, but the cracking initiation load is only marginally augmented since reinforcement mechanisms of fibres are mainly activated after they have been crossed by a crack. The composite material's toughness is significantly enhanced due to the additional energy required for pulling out the fibres crossing a crack (Cunha *et al.* 2010). Fibres bridging the cracks have the ability of modifying the concrete softening response, which influence the cracking and deflection behaviour of concrete structures (de Montaignac *et al.* 2012). Steel fibres are still the most vastly used for the concrete reinforcement due to their stiffness and readiness of being provided with geometric features that ensure efficient anchorage mechanisms mobilized during the fibre pullout (Wu *et al.* 2021). Due to the above advantages, SFRC is becoming increasingly popular in the construction industry.

For ordinary concrete, knowledge of compressive strength is generally sufficient to establish credibly other material characteristics (tensile strength, elasticity and shear modulus, fracture energy, creep factor, shrinkage strain, etc.) that are necessary for the analysis of RC structures in practice. However, SFRC requires additional tests to assess its post-cracking tensile behaviour. Due to a large variety of fibres (shape, length, diameter, strength, etc.) and concrete characteristics, and considering the highly complex nature

*Corresponding author, Professor
E-mail: gintaris.kaklauskas@vilniustech.lt
[a]Senior Research Fellow
E-mail: aleksandr.sokolov@vilniustech.lt
[b]Ph.D. Candidate
E-mail: ashkan.shakeri@gmail.com
[c]Senior Research Fellow
E-mail: irdngpl@gmail.com
[d]Professor
E-mail: barros@civil.uminho.pt

ISSN: 1225-4568 (Print), 1598-6217 (Online)

of interaction between fibres and concrete, the post-cracking tensile behaviour of SFRC is generally assessed by performing mechanical tests with SFRC specimens (Amin *et al.* 2017). The post-cracking tensile behaviour of SFRC is generally assessed by determining residual strength parameters, like the ones proposed by *fib* Model Code 2010 (2013), or the stress-crack width relation, from which the residual stress at different crack width values can be determined, as well as the mode I fracture energy of the SFRC.

Among the experimental techniques, the uniaxial tensile test is recognised to be the most direct and adequate method for establishing the stress-crack width relation (Stähli 2008, Amin *et al.* 2017). However, this technique is complex and time-consuming as it is associated with sophisticated testing equipment and meticulous preparation of test specimen. Therefore, the uniaxial tests are rather rarely used in practice (Amin *et al.* 2015). The indirect methods such as bending tests, splitting tensile tests (Abrishambaf *et.al.* 2015, ASTM C496-17 2017), wedge splitting tests (Skocek and Stang 2008) or round panel tests (Soltanzadeh *et al.* 2019, Minelli and Plizzari 2015) are simpler, and therefore more preferable by the practitioners. Among the indirect methods, the bending tests are most widely used for determining the residual strength of SFRC due to the simplicity of the testing equipment and the specimen preparation. The bending tests are codified in various design standards (RILEM TC 162-TDF 2000, EN 14651 2005, ASTM C1609/C1609M-12 2012, UNI 11039 2003, JSCE. SF4 1984, DAfStb 2012). RILEM (2000) proposed a three-point notched beam bending test to determine the equivalent flexural tensile strength parameters (f_{eq2} and f_{eq3}) considering the areas under the load-deflection diagram, from which the post-cracking tensile behaviour can be defined. The flexural stress versus crack mouth opening displacement (CMOD) can also be obtained from this test, where the CMOD can be recorded by a displacement sensor, or evaluated from an equation that relates the CMOD with the beam's deflection (Cunha 2010). Based on the flexural stress versus CMOD relation derived from this type of test, Model Code 2010 (2013) has proposed a methodology (similar to the one already indicated by RILEM (2000)) for determining the residual flexural tensile strength parameters, f_{Ri} (i=1 to 4) that are used to classify the toughness class of SFRC. Furthermore, the equivalent flexural tensile strength parameters (f_{eq2} and f_{eq3}) and the residual flexural tensile strength parameters (f_{R1} and f_{R3}) are used for defining the constitutive laws of SFRC for the verifications of serviceability and ultimate limit states (abbreviated as SLS and ULS, respectively) design requirements. RILEM (2001) described a test to evaluate the relationship between uniaxial stress and crack opening, which was incorporated in a recommended design procedure (RILEM 2002). RILEM (2003) also suggested a σ-ε design method for SFRC sections under flexure by using the f_{eq} or f_{Ri}. European Standard EN 14651 (2005) proposes the concept of f_{Ri} of SFRC material for design purposes at SLS and ULS. German Guideline DafStb (2012) classified the design of SFRC members in two performance levels: level 1 for small deformations; and level 2 for large deformations considering the combination of reinforcement (fibres and conventional reinforcements).

In most structural applications, fibres are used along with longitudinal reinforcement bars. In this study, such structural members are designated by the acronym R/SFRC. Serviceability analysis of these members is rather complex due to the sophisticated behaviour of the tension zone of the members (Harvinder 2020, Lehmann and Głodkowska 2021). Concrete cracking mobilizes two types of tensile stresses of different nature. Tension softening stresses are one of these types, herein known as residual stresses, which develop in the cracked sections of SFRC as a result of the bridging stress mechanisms provided by fibres crossing these sections. The tension stiffening stresses are the other type of tensile stresses, which are generated in the portions of the structural member between the cracks due to the bond interaction between reinforcement bars and surrounding concrete. Numerous investigations have been carried out on tension stiffening in several approaches, namely:

Semi-empirical models, which are the earliest approaches based on the simple formulae of strength of materials and the effective geometric characteristics of a cross-section adjusted to the test data (e.g., ACI 544.4R-88 1988). This type of approaches are frequently used in simplified structural design methods;

Stress transfer models that aim to model the bond between the tensile steel bars and surrounding concrete. Models based on the bond stress-slip mechanism are able to realistically deal with discrete cracking phenomenon (Lackner and Mang 2003, Wu and Gilbert 2009). The numerical results are mainly governed by the chosen bond-slip model;

Concrete-related stress-strain models, which due to its simplicity, are widely used in numerical analysis (Torres *et al.* 2004, Ng *et al.* 2010). Kaklauskas and Ghaboussi (2001) proposed an inverse technique for deriving the tension stiffening law from the moment-curvature diagrams recorded in the experimental tests with RC members. The inverse technique was applied to R/SFRC beams (Gribniak *et al.* 2012), and was further developed by removing the shrinkage effect from moment-curvature and tension stiffening relations (Kaklauskas and Gribniak 2011);

Reinforcement-related stress-strain models, such as the case of the one proposed by Gilbert and Warner (1978) are rarely applied. This approach assumes that the tensile reinforcement is capable of taking additional stresses due to the tension stiffening effect. It has been further developed by Kaklauskas *et al.* (2011) and Torres *et al.* (2015). An analytical inverse technique for constitutive modelling of the tension stiffening phenomenon considering the shrinkage effect was suggested by Kaklauskas and Gribniak (2016);

Fracture mechanics: this approach is based on the fracture mechanics principles to predict cracking behaviour of RC elements (Bertram 1999, Shi 2009). The models based on this type of approach are able to provide high fidelity solutions of localised effects, and are often used in combination with other approaches.

The deformational behaviour of SFRC structural members has been the subject of numerous research works.

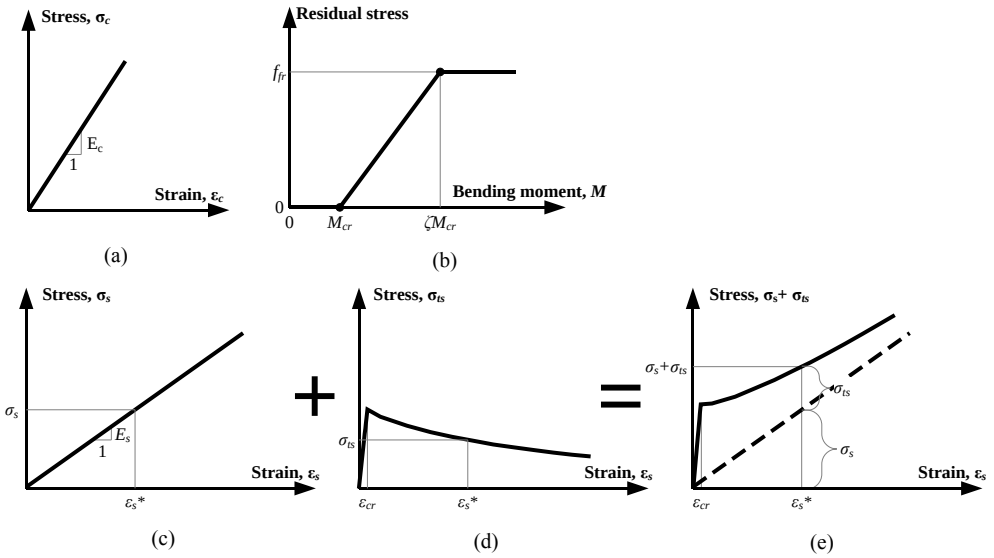

Fig. 1 Constitutive laws for modelling the: (a) compressive concrete; (b) residual stress in tensile concrete; (c) tensile reinforcement; (d) fictitious tension stiffening stress acting in the reinforcement; and (e) fictitious total stress acting in the reinforcement

Simplified methods of deflection analysis of R/SFRC beams falling into the category of the *semi-empirical models* were proposed by Craig (1987), Lim *et al.* (1987) and Hsu *et al.* (1992). Alsayed (1993) reported test results of 10 reinforced concrete beams with and without steel fiber reinforcement and proposed a simple empirical equation to estimate deflection. Ashour and Wafa (1993) reported test results on eight high-strength concrete (88 MPa) beams with different fibre contents. A semi-empirical equation was proposed to estimate the effective moment of inertia of simply supported high-strength fiber reinforced concrete beams. Tan *et al.* (1994) proposed a modification of the Branson method to calculate the effective moment of inertia for R/SFRC beams. Ezeldin and Shiah (1994) presented a method for the calculation of SFRC beam deflection both under instantaneous and long term loads. A review of simplified methods for deflection analysis of R/SFRC members was presented by Domski and Zakrzewski (2020).

Amin *et al.* (2015) have experimentally assessed the post-crack resistance of SFRC elements without steel reinforcement under flexure, and compared the results with the load response of beams containing both steel bar and fibre reinforcement (Amin *et al.* 2017, Amin and Gilbert 2018). Based on the experimental load response, they proposed a model for predicting deflection of R/SFRC beams by modifying the model from Marti *et al.* (1998). Based on experimental results of R/SFRC beams and slabs reinforced with different fibre volumes, Barros and Figueiras (1999) proposed a layered model for predicting the moment-curvature relationship of this type of elements, from which their force-deflection response can be derived by using the secant or the tangent flexural stiffness. Campione (2008) proposed a model for predicting the flexural strength of R/SFRC beams under pure bending conditions. This simplified method allowed the evaluation of load-displacement diagrams by means of linear interpolation between three characteristic points corresponding to cracking, yielding and ultimate loads, while the tension-stiffening effect was neglected. Montaignac *et al.* (2012) proposed a model for predicting the behaviour of SFRC members under bending. A comprehensive experimental investigation was performed on rectangular and T-shape section R/SFRC beams having fibres of various types in terms of material and geometric characteristics. The study assessed the fibre reinforcement contribution to resist the external load, and presented a practical design provision for T-shape SFRC beams. Mazaheripour *et al.* (2016) developed a model to predict the deflection and crack width of I-shape SFRC beams that include passive or prestressed flexural reinforcement formed by steel and fibre reinforced polymer (FRP) bars, while fibres are used in an attempt of replacing integrally steel stirrups. This model also considers the shear stiffness degradation effect during the crack opening process on the deflection of this type of R/SFRC beams.

The present paper describes the analytical technique developed for estimating the flexural deformation response of R/SFRC members. The tension stiffening effect is considered via the reinforcement-related approach. The resultant internal force due to the tension stiffening is assumed from the analogy of an equivalent RC member with the same geometry and materials (except the explicit participation of the fibres) having the same reinforcement strain level at the cracked section. The mean strain value in the tensile reinforcement of the RC member is evaluated per the *fib* Model Code 2010 (2013) provisions. The post-cracking tensile capacity of SFRC is assumed constant within the tension zone at SLS condition with the magnitude of the residual stress taken from a simple existing model that does not require any test results on the tension or bending behavior of SFRC. Thus, the need of dedicated mechanical testing for individual design cases is circumvented. To validate the proposed technique, R/SFRC beam specimens tested in the literature are selected for

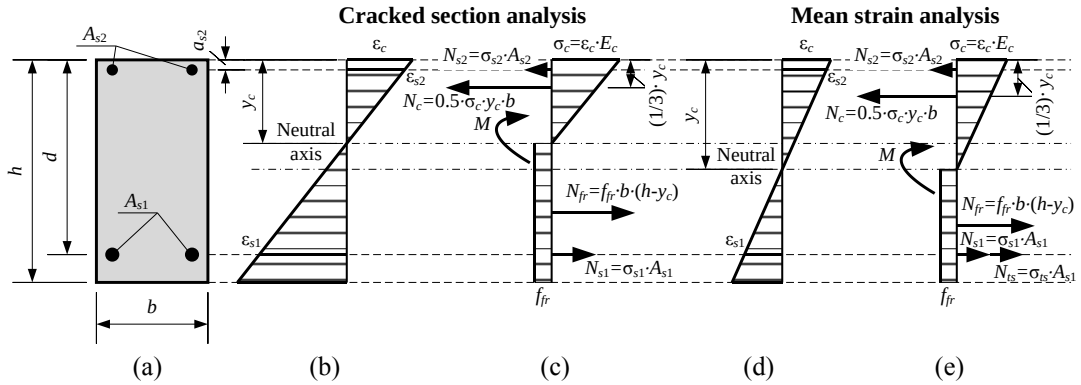

Fig. 2 Doubly reinforced section subjected to external bending: (a) cross-section; (b) strain compatibility for cracked section analysis; (c) stresses, internal forces and external bending moment acting in the cracked section; (d) strain compatibility for mean strain analysis; (e) stresses, internal forces and external bending moment for mean strain analysis

analysis, and the moment-curvature relations predicted from the proposed inverse technique are compared to those obtained experimentally. The current study also introduces the concept of *effective* residual stress, whose detailed description will be provided in Section 6.

2. Assumptions and governing equations

2.1 Assumptions and constitutive laws

The developed approach aims to determine curvatures of concrete bending members reinforced with steel bars and fibres (R/SFRC members). This approach is based on the constitutive laws depicted in Fig. 1 and on the following assumptions:

1. Under flexural deformation, the member cross-section remains plane and has linear strain distribution along its depth. This hypothesis is applied for strain field at a cracked section and for the cross sections spanning over a sufficient length for forming several cracks in order to be representative of a region at stabilized cracking conditions (average strain concept is used in this case);

2. Reinforcements and concrete in compression behave as linear-elastic materials (Fig. 1(a), (c)). This assumption is close to reality since the structural member is considered under service condition;

3. Fibres have no influence on the concrete behaviour in compression. The effect of fibres on the tensile behaviour of concrete is activated when bending moment reaches the cracking initiation, M_{cr} (Fig. 1(b)). The effect is considered via the residual stress of SFRC by assuming this composite behaves as a tensile strain softening material, since it is the most current class in structural applications;

4. A rectangular stress block with a constant residual stress value is taken within the tension zone up to the neutral axis (Barros *et al.* 2017);

5. Within the early stages of cracking, the residual tensile stress increases linearly from zero to its value f_{fr} proportionally to the bending moment ranging between M_{cr} and ζM_{cr} (see Fig. 1(b)). The physical justification behind this assumption is that each new crack in the crack formation stage induces tension softening stresses that gradually contribute to the stiffness of the structure. When the loading exceeds ζM_{cr}, the residual stress is taken constant as f_{fr};

6. In addition to the residual stress, tension stiffening is taken into account as another independent effect of the tensile zone contributing to the stiffness of the R/SFRC member;

7. Tension stiffening is assessed via the reinforcement-related approach (Fig. 1(c)-(e)). It supposes that the tensile reinforcement in addition to the actual stress is capable of taking fictitious stress due to the tension stiffening effect. Tension stiffening stresses act in the area of tensile reinforcement with their resultant force N_{ts} positioned at the centroid of the reinforcement. Tension stiffening is modelled by fictitious stress-strain relation (Fig. 1(d)) that can be quantified by the inverse approach based on the moment-curvature response;

8. The tension stiffening effect is estimated based on the analogy of a R/SFRC member and the equivalent RC member having equal geometry and materials except the explicit participation of fibres. It is assumed that the resultant tension stiffening force of the R/SFRC member can be calculated as for the equivalent RC member providing that the reinforcement strain in the cracked section of these members is the same, ε_{si}. This assumption is illustrated in Fig. 3 and is discussed in more detail in Section 3.

2.2 Equilibrium equations

In order to derive the equilibrium equations, a concrete rectangular cross section member subjected to bending with longitudinal reinforcement in tension and compression zone is considered, as depicted in Fig. 2(a). Fig. 2 also shows schematic diagrams of strain and stress distribution across the section with respective resultant internal forces and bending moment for two distinct phases of analysis, as will be detailed in Subsection 2.3:

a) Cracked section analysis (Fig. 2(b), (c)). The effect of tension stiffening is neglected, N_{ts}=0, refer to Fig. 2(c).

b) Mean strain analysis (Fig. 2(d), (e)) dealing with average deformations at cross sections over a length spanning across several cracks. The effect of tension

stiffening is taken into account, with the tension stiffening resultant $N_{ts}\neq 0$, refer to Fig. 2(e).

It should be kept in mind that the only characteristic making a distinction between the two analyses is whether the tension stiffening force is taken to be zero or not. Although these analyses will result in different prediction outcomes (curvatures, strains and stresses), for sake of generalisation and simplicity of presentation, notations of the parameters involved in the equilibrium equations will be taken the same. The equilibrium equations of axial forces and bending moments with respect to the centroid of the compressive concrete are written for the general case, when $N_{ts}\neq 0$, as illustrated in Fig. 2(e)

$$N_c + N_{s2} - N_{fr} - N_{s1} - N_{ts} = 0 \tag{1}$$

$$M + N_{s2}\left(\frac{y_c}{3} - a_{s2}\right) - N_{fr}\left(\frac{h-y_c}{2} + \frac{2}{3}y_c\right) - (N_{s1} + N_{ts})\left(d - \frac{y_c}{3}\right) = 0 \tag{2}$$

where y_c is the depth of neutral axis; N_{fr} is the resultant force of residual tensile stresses; and N_{s1}, N_{s2} and N_c are the internal forces acting in tension and compression reinforcement and in the compressive concrete, respectively. For simplicity, the residual tensile stress, denoted by f_{fr}, is assumed to be uniformly distributed over the tension zone (according to the aforementioned Assumption 4), as shown in Fig. 2(c). From Eqs. (1) and (2), the internal forces can be expressed through the respective stresses, as given by Eqs. (3) and (4)

$$\frac{1}{2}by_c\sigma_c + A_{s2}\sigma_{s2} - f_{fr}b(h-y_c) - A_{s1}\sigma_{s1} - N_{ts} = 0 \tag{3}$$

$$M = (N_{ts} + A_{s1}\sigma_{s1})\left(d - \frac{y_c}{3}\right) - A_{s2}\sigma_{s2}\left(\frac{y_c}{3} - a_{s2}\right) + f_{fr}b(h-y_c)\left(\frac{h-y_c}{2} + \frac{2}{3}y_c\right) \tag{4}$$

Denote the tension steel strain by ε_{s1}, compression steel strain by ε_{s2}, and concrete strain at extreme compression fibre by ε_c. Considering the plane section hypothesis, the values of ε_c and ε_{s2} can be obtained by Eqs. (5) and (6), respectively

$$\varepsilon_c = \frac{y_c}{(d-y_c)}\varepsilon_{s1} \tag{5}$$

$$\varepsilon_{s2} = \frac{(y_c-a_{s2})}{(d-y_c)}\varepsilon_{s1} \tag{6}$$

Stresses in the compressive concrete, as well as tensile and compressive reinforcement, can be calculated from the following equations

$$\sigma_c = E_c\varepsilon_c \tag{7}$$

$$\sigma_{s1} = E_{s1}\varepsilon_{s1} \tag{8}$$

$$\sigma_{s2} = E_{s2}\varepsilon_{s2} \tag{9}$$

2.3 Two main stages of analysis

In general terms, the curvature analysis by the proposed approach is performed through two main stages corresponding to the above cases of analysis:

1) Cracked section analysis (Fig. 2(b), (c)). The constitutive laws for compressive concrete and reinforcement are shown in Fig. 1(a) and (c), respectively. After a section reaches cracking load, tensile concrete carries residual stresses (Fig. 1(b)). The tension stiffening effect is obviously not present for the cracked section. Solving the equilibrium Eqs. (3) and (4) under the condition of $N_{ts}=0$ will result in determining two unknowns: depth of the neutral axis, y_c, and tensile reinforcement strain, ε_{s1}. The latter will be used in the second stage to calculate the tension stiffening resultant, N_{ts}.

2) Mean strain analysis (Fig. 2(d), (e)). The constitutive laws for compressive and tensile concrete are shown in Fig. 1(a) and 1(b), respectively. As illustrated in Fig. 1(d) and 1(e), tension stiffening is attributed to the tensile reinforcement. Thus, according to Assumption 7, the tensile reinforcement in addition to its actual stress (Fig. 1(c)) is capable of carrying fictitious tension stiffening stress (Fig. 1(d)). As an illustration of the general case, Fig. 1(e) depicts the fictitious total stress acting in the tensile reinforcement. For a given reinforcement mean strain, ε_s^*, fictitious total stress (Fig. 1(e)) can be calculated as the sum of actual stress (Fig. 1(c)) and fictitious tension stiffening stress (Fig. 1(c)). It should be noted that the constitutive laws of tension stiffening shown in Fig. 1(d) and 1(e) represent mean stresses and strains.

For this case, the two equilibrium equations hold three unknowns: depth of the neutral axis y_c, mean strain of tensile reinforcement ε_{s1} and tension stiffening resultant N_{ts}. To reduce the number of unknowns to two, N_{ts} is obtained based on Assumption 8 and the concept of the equivalent RC member using the reinforcement strain in the cracked section calculated in the first stage. Calculation of N_{ts} and steps of analysis by the proposed approach will be described in detail in Sections 3 and 4, respectively.

On the basis of Eqs. (3) to (9), the depth of neutral axis can be determined as the solution of the quartic (fourth-order) equation given by Eq. (10), where the polynomial coefficients C_0 to C_4 may be computed via Eqs. (11) to (15), respectively. The solution process of quartic equation is contained in Appendix A.

$$C_4y_c^4 + C_3y_c^3 + C_2y_c^2 + C_1y_c + C_0 = 0 \tag{10}$$

$$C_0 = -12ME_{s2}A_{s2}a_{s2} + 12f_{fr}E_{s2}A_{s2}hba_{s2}^2 + 12N_{ts}E_{s2}A_{s2}da_{s2} + 6f_{fr}E_{s2}A_{s2}bh^2a_{s2} + 12N_{ts}E_{s2}A_{s2}a_{s2}^2 - 12ME_{s1}A_{s1}d + 6f_{fr}E_{s1}A_{s1}bdh^2 - 12f_{fr}E_{s1}A_{s1}bhd^2 \tag{11}$$

$$C_1 = 12ME_{s1}A_{s1} - 6f_{fr}E_{s2}A_{s2}bh^2 - 6f_{fr}E_{s1}A_{s1}bh^2 - 12N_{ts}E_{s2}A_{s2}d - 20N_{ts}E_{s2}A_{s2}a_{s2} - 20f_{fr}E_{s2}A_{s2}bha_{s2} - 12f_{fr}E_{s2}A_{s2}ba_{s2}^2 + 12ME_{s2}A_{s2} + 12f_{fb,r}E_{s1}A_{s1}bhd + 12f_{fr}E_{s1}A_{s1}bd^2 \tag{12}$$

$$C_2 = 6ME_cb - 3f_{fr}E_ch^2b^2 - 18f_{fr}E_{s1}A_{s1}bd + 14f_{fr}E_{s2}A_{s2}ba_{s2} + 8f_{fr}E_{s2}A_{s2}bh - 6N_{ts}E_cbd + 8N_{ts}E_{s2}A_{s2} \tag{13}$$

$$C_3 = 2f_{fr}E_chb^2 + 6f_{fr}E_{s1}A_{s1}b - 2f_{fr}E_{s2}A_{s2}b + 2N_{ts}E_cb \tag{14}$$

$$C_4 = f_{fr}E_cb^2 \tag{15}$$

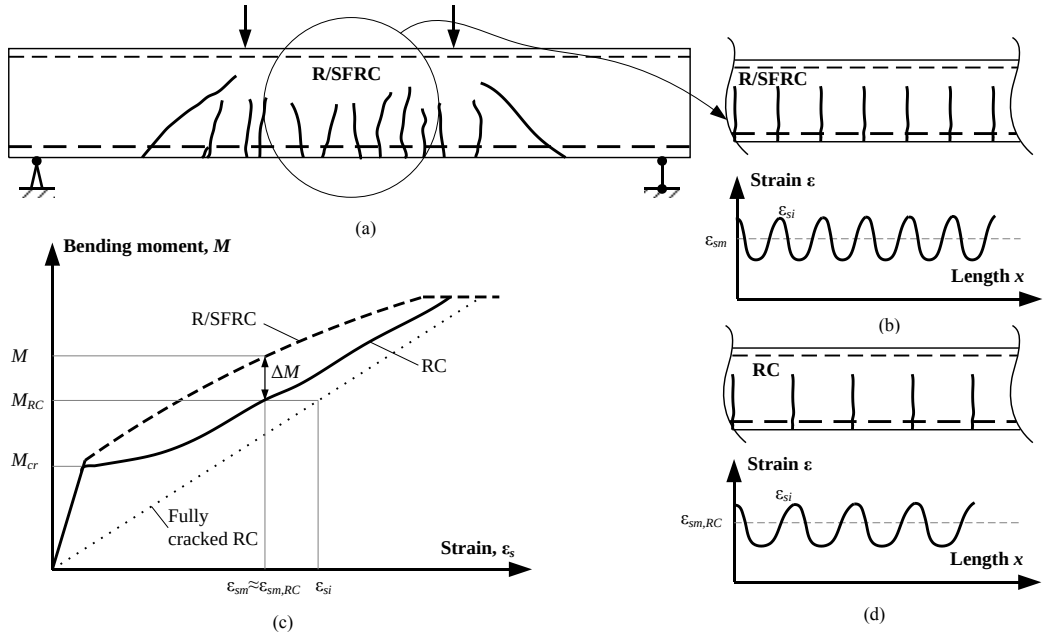

Fig. 3 Details of curvature analysis: (a) a crack pattern of R/SFRC beam; (b) a fragment of R/SFRC beam and the tensile reinforcement strain profile; (c) establishment of bending moment M_{RC} corresponding to reinforcement strain ε_{si} in the equivalent RC beam; (d) a fragment of the equivalent RC and the tensile reinforcement strain profile

2.4 Residual tensile stress

Knowledge of the residual tensile stress f_{fr} is required for establishing the coefficients of the quartic equation. Due to highly complex behaviour of cracked SFRC, very few theoretical models were proposed for defining the residual strength. In codified design practices, the residual stress needs to be quantified by means of standard bending tests. Naaman (2003) proposed a semi-empirical method for determining the residual stress in SFRC members, and the method was further modified by Campione *et al.* (2006). According to Naaman (2003), the residual stress is given by Eq. (16)

$$f_{fr,Naaman} = \lambda_1\lambda_2\lambda_3\tau\, V_f\, \frac{l}{d_f} \tag{16}$$

where λ_1 is a coefficient reflecting the expected normalized fibre pull-out length calculated as the ratio of the statistically defined fibre embedment length (l/4) over the fibre length, λ_2 is the efficiency factor of fibre orientation in the cracked state, λ_3 is the group reduction factor associated with the number of fibres pulling-out per unit area (or density of fibre crossings), τ is the average bond stress developed in a single fibre embedded in concrete, l, d_f, and V_f are the length, diameter and volume fraction of fibres, respectively. Naaman (2003) suggested the values of λ_1=0.25, λ_2=1.2 and λ_3=1.0 and to the average bond stress as τ=2f_{ct}, where f_{ct} is the mean tensile strength of concrete. These suggestions are adopted in the present study.

Campione *et al.* (2006) introduced a coefficient β that reflects the bond characteristics of different fibre types and suggested to use the values of 0.5 for smooth fibres, 0.75 for crimped fibres and 1.0 for hooked fibres. By way of the above, the residual tensile stress of SFRC can be obtained from Eqs. (17) and (18)

$$f_{fr,modified} = 2\lambda_1\lambda_2\lambda_3 f_{ct} F \tag{17}$$

$$F = V_f\, \frac{l}{d_f}\beta \tag{18}$$

in which F is referred to as the fibre factor. In this study, Eqs. (17) and (18) are employed for the evaluation of f_{fr}. Further, as discussed in Assumption 5 above, for the load stage $M \geq \zeta M_{cr}$ the residual stress is directly taken as f_{fr}. Whereas at the load interval $\zeta M_{cr} > M \geq M_{cr}$ the residual stress should be linearly interpolated between 0 and f_{fr} proportionally to the bending moment ranging from M_{cr} to ζM_{cr}. Based on the above, the residual stress is taken as

$$f_{fr} = \begin{cases} f_{fr,modified}, & \text{when } M \geq \zeta M_{cr} \\ f_{fr,modified} \cdot \frac{M - M_{cr}}{(\zeta - 1)M_{cr}}, & \text{when } M_{cr} \leq M < \zeta M_{cr} \end{cases} \tag{19}$$

In the current study, it is assumed that ζ=2, and the cracking moment is calculated as M_{cr}=$f_{ct}bh^2$/6 per design standard *fib* Model Code 2010 (2013).

3. Determination of reinforcement-related tension-stiffening force

The analytical procedure developed herein aims at calculating the tension stiffening force in R/SFRC members. It is based on Assumptions 7 and 8 and the inverse analysis approach reported in (Kaklauskas *et al.* 2011, Torres *et al.* 2015, Kaklauskas and Gribniak 2016). The latter is dedicated to the constitutive modelling of tension stiffening derived from the moment-curvature response of RC beam. Assumption 7 asserts that the tension stiffening effect is modelled by fictitious mean stress-mean strain relation attributed to the tensile reinforcement. It postulates that tension stiffening stresses act in the area of

Table 1 Notations for strain of tensile reinforcement

Type of analysis	Member	
	R/SFRC	RC
Cracked section analysis, N_{ts}=0	$\varepsilon_{s1}=\varepsilon_{si}$	
Mean strain analysis, $N_{ts}\neq 0$	$\varepsilon_{s1}=\varepsilon_{sm}$	$\varepsilon_{s1}=\varepsilon_{sm,RC}$

tensile reinforcement with their resultant force N_{ts} acting at the centroid of the reinforcement.

Assumption 8 permits relating the tension stiffening forces N_{ts} in the RC and R/SFRC members. For that, the term *equivalent RC beam* is introduced to characterize the RC beam having similar geometry and materials (except the steel fibres are absent) to that of the R/SFRC beam. It is postulated that the fibre contribution to the tensile resistance of a cracked R/SFRC member is fully reflected by the residual stress. Consequently, the tension stiffening force N_{ts} is the same for an R/SFRC element and the equivalent RC member providing that the strains of the tensile reinforcement in the cracked section of both members are equal.

The suggested approach of analysis is illustrated in Fig. 3. It shows the considered R/SFRC beam (Fig. 3(a)) and the reinforcement strain distribution in the SFRC beam (Fig. 3(b)) and in the equivalent RC beam (Fig. 3(d)). These figures illustrate the strain in the cracked section ε_{si} and the mean reinforcement strain ε_{sm}. It should be kept in mind that in the equilibrium Eqs. (3) and (4) strains ε_{si} and ε_{sm} will stand as ε_{s1}. To facilitate the perception of this aspect, strain notations of tensile reinforcement for R/SFRC and RC members are summarised in Table 1. Extra subscript "RC" refers to the *equivalent* RC beam. Fig. 3(c) shows the moment-curvature diagrams for the considered R/SFRC and the *equivalent* RC beams with respective bending moments M and M_{RC} ($M_{RC}<M$) inducing the same reinforcement strain ε_{si} in the cracked sections of the members.

After calculating the reinforcement strain $\varepsilon_{s1}=\varepsilon_{si}$ in the cracked section of the R/SFRC member using Eqs. (3) to (4) and the condition N_{ts}=0, bending moment M_{RC} inducing the same reinforcement strain ε_{si} in the *equivalent* RC beam can be defined by this expression relating moment to reinforcement strain of the fully cracked section (Mazaheripour 2016)

$$M_{RC} = \varepsilon_{si}\frac{E_c I_{cr}}{(d-y_{c,RC})} \tag{20}$$

where $y_{c,RC}$ and I_{cr} are, respectively, the compressive depth and the moment of inertia of the fully cracked RC section. These geometrical characteristics are calculated using the following equations

$$y_{c,RC} = \sqrt{\left(\frac{(n-1)A_{s2}+nA_{s1}}{b}\right)^2 + \frac{2((n-1)A_{s2}a_{s2}+nA_{s1}d)}{b}} - \frac{(n-1)A_{s2}+nA_{s1}}{b} \tag{21}$$

$$I_{cr} = \frac{y_{c,RC}{}^3 b}{3} + (n-1)\left(y_{c,RC}-a_{s2}\right)^2 A_{s2} + n(d-y_{c,RC})^2 A_{s1} \tag{22}$$

where $n=E_s/E_c$ is the modular ratio.

Further, the main equations for deriving the tension stiffening force N_{ts} at a given bending moment are presented. Consider the equilibrium of axial forces and bending moments of the RC beam section as shown in Fig. 2, and taking the residual tensile force N_{fr}=0, Eqs. (23) and (24) can be obtained

$$N_{ts} + N_{s1} - N_c - N_{s2} = 0 \tag{23}$$

$$N_c\left(d-\frac{y_c}{3}\right) + N_{s2}(d-a_{s2}) - M_{RC} = 0 \tag{24}$$

Solving Eqs. (23) and (24), the value of tension-stiffening force N_{ts} is obtained as expressed in Eq. (25) (*fib* Model Code 2010 (2013))

$$N_{ts} = \kappa_m\left[\frac{E_c y_c{}^2 b}{2A_{s1}} + (E_{s2}-E_c)(y_c-a_{s2})\frac{A_{s2}}{A_{s1}} - E_{s1}(d-y_c)\right]A_{s1} \tag{25}$$

where κ_m is the mean curvature of the *equivalent* RC member corresponding to M_{RC}. The procedure for calculating the neutral axis depth $y_{c,RC}$ for the equivalent RC beam is described in Appendix B.

The fictitious tension stiffening stress is assessed as

$$\sigma_{ts} = \frac{N_{ts}}{A_{s1}} \tag{26}$$

The mean curvature κ_m is calculated for the value of bending moment $M=M_{RC}$ (see Fig. 3(c)) according to the Model Code 2010 (2013) technique by this interpolation formula

$$\kappa_m = (1-\zeta)\kappa_{el} + \zeta\kappa_{cr} \tag{27}$$

where κ_{el} and κ_{cr} are the curvatures of the uncracked and fully cracked sections, and ζ is the distribution coefficient that is determined by Eq. (28) for cracked sections (the value of ζ is zero if the section is uncracked, i.e., $M\leq M_{cr}$).

$$\zeta = 1 - \left(\frac{M_{cr}}{M}\right)^2 \tag{28}$$

in which the curvature of the cracked section κ_{cr} can be calculated per Eq. (29)

$$\kappa_{cr} = \frac{M}{E_c I_{cr}} \tag{29}$$

where I_{cr} is the moment of inertia of the cracked RC beam and can be obtained from Eq. (22), and the elastic curvature of the uncracked section κ_{el} is defined by Eq. (30)

$$\kappa_{el} = \frac{M}{E_c I_{el}} \tag{30}$$

where I_{el} is the moment of inertia of the uncracked RC member and is simply obtained from Eq. (31)

$$I_{el} = \frac{bh^3}{12} \tag{31}$$

It should be noted that the current study has not provided proof of Assumption 8. Quantification of tension stiffening in R/SFRC members by decoupling residual strength and tension stiffening is a highly complex issue, as evidenced in Mazaheripour *et al.* (2016). As a mean crack spacing in the R/SFRC member is smaller than the one in the *equivalent* RC member, it could be supposed that the integral of the bond stresses along the bar (and the tension stiffening effect) will be also smaller in the R/SFRC member. However, the experimental investigations of bond-

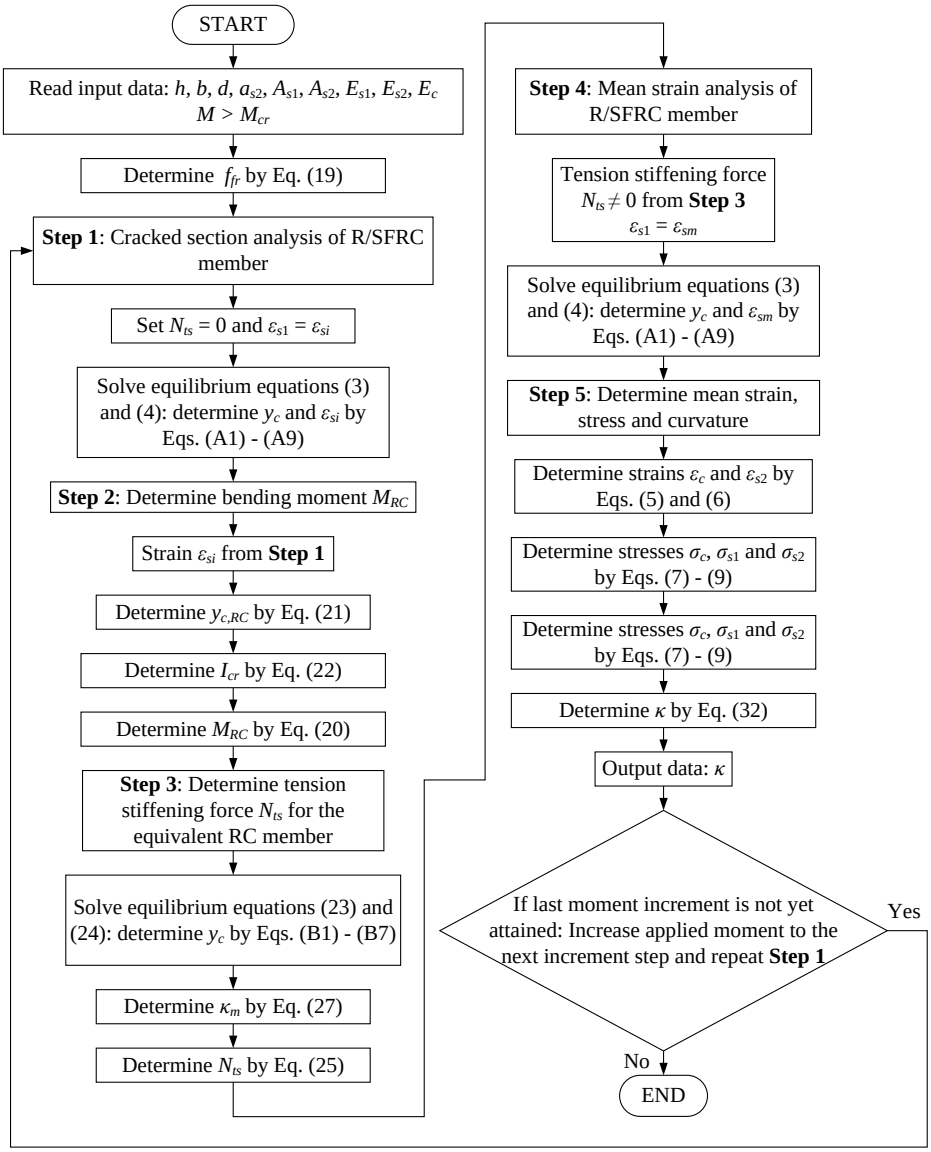

Fig. 4 Flowchart of curvature analysis of a R/SFRC member subjected to bending

slip in SFRC have demonstrated (Chu and Kwan 2021) that mean bond stress and bond stiffness increase by adding steel fibres. Moreover, steel fibers restrain the splitting cracks in the vicinity of primary cracks that also contributes to the mean bond stress of the R/SFRC member. As a result, it is very difficult to speculate about the fidelity of Assumption 8. Until further investigations are conducted in this regard, the current study takes Assumption 8 along with simplified models of tension stiffening (Eq. (27)) and residual strength (Eq. (17)).

4. Moment-curvature analysis of R/SFRC flexural members

Stepwise calculation is adopted for the moment-curvature analysis. To capture the nonlinear moment-curvature response, the total external moment is applied to the R/SFRC member in incremental steps. As shown in a flowchart given in Fig. 4, the curvature analysis of the deformed member is performed through the following steps:

Step 1. For the given bending moment M, the section analysis is performed at the cracked section of the SFRC member. Reinforcement strain $\varepsilon_{s1}=\varepsilon_{si}$ is established from the equilibrium Eqs. (3) and (4) assuming $N_{ts}=0$. It should be noted that among the four roots of the quartic equation (Eqs. (10) to (15)), y_c is obtained as the real positive root, while the negative and imaginary roots are rejected (refer to Appendix A). The value of root is then substituted in lieu of y_c in Eqs. (3) or (4), so that the other unknown, i.e., $\varepsilon_{s1}=\varepsilon_{si}$, can be obtained.

Step 2. The bending moment M_{RC} corresponding to the reinforcement strain in the cracked section ε_{si} of the *equivalent* RC member (see Fig. 3(c),(d)) is assessed based on Eq. (20) (Kaklauskas *et al.* 2014).

Step 3. The tension stiffening force N_{ts} is calculated for the *equivalent* RC member based on Eq. (25), and the curvature in the RC beam is obtained by using the Model Code recommendations with the deformation parameter set

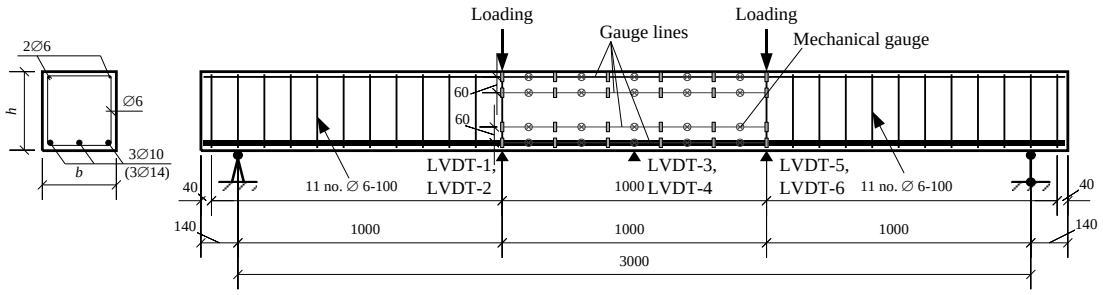

Fig. 5 Dimensions and reinforcement layout of beams (dimensions in mm)

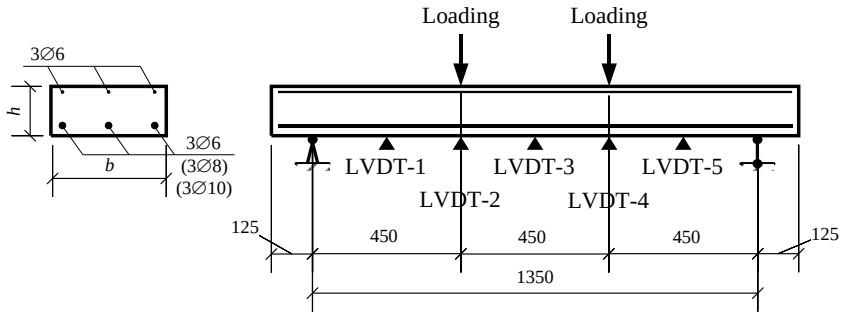

Fig. 6 Dimensions and reinforcement layout of slab strips (dimensions in mm)

Table 2 Main characteristics of R/SFRC specimens analysed

Specimen	h	b	d	a_{s2}	A_{s1}	A_{s2}	ρ_{s1}	ρ_{s2}	f_{sy}	E_s	f_{cm}	V_f
	mm				mm^2		%	%	MPa	GPa	MPa	%
S2-F05	301	286	273	25	477	56	0.55	0.07	559	205.3	55.6	0.47
S2-F10	301	283	272	22	477	56	0.56	0.07	559	205.3	48.0	1.02
S2-F15	299	284	272	23	477	56	0.56	0.07	559	205.3	52.2	1.46
S3-1-F05	302	278	278	29	235	56	0.28	0.07	606	208.8	55.6	0.47
S3-2-F05	303	283	279	26	235	56	0.27	0.07	606	208.8	55.6	0.47
S3-1-F10	300	279	276	23	235	56	0.28	0.07	606	208.8	48.0	1.02
S3-2-F10	301	284	275	25	235	56	0.27	0.07	606	208.8	48.0	1.02
S3-1-F15	300	279	272	26	235	56	0.28	0.07	606	208.8	52.2	1.46
S3-2-F15	299	285	273	23	235	56	0.28	0.07	606	208.8	52.2	1.46
A-6-45	150	350	127	23	85	85	0.19	0.19	568	200.0	99.2	0.57
B-8-45	150	350	126	23	151	85	0.34	0.19	585	200.0	99.2	0.57
C-10-45	150	350	125	23	236	85	0.54	0.19	591	200.0	99.2	0.57

as the curvature, Eqs. (27) to (31) refer.

Step 4. With respect to the established value of N_{ts}, the mean deformation analysis of the R/SFRC member is performed (Fig. 2(b) and 2(e)). The equilibrium equations are again solved for updated values of ε_{s1}=ε_{sm} (by taking into account the tension stiffening effect) and y_c, following the similar solution process of the quartic equation as described in Step 1.

Step 5. The mean strain values ε_c and ε_{s2} are computed from Eqs. (5) and (6). Mean stresses in the compressive concrete and tensile and compressive reinforcement are calculated from Eqs. (7) to (9). By Assumption 1 (plane section remains plane in the deformed beam), the strain distribution along the depth of cross-section is linear. Therefore, the curvature can be computed using Eq. (32)

$$\kappa = \frac{\varepsilon_{s1}+\varepsilon_c}{d} = \frac{\varepsilon_c}{y_c} = \frac{\varepsilon_{s1}}{d-y_c} \tag{32}$$

Step 6. The applied moment M is increased to the value of the next increment step, and the above Steps 1 to 5 are repeated until the last moment increment is attained.

5. Comparison of curvature prediction to the test results

This section validates the proposed analytical technique and illustrates its application to the simulation of the test moment-curvature response of R/SFRC members. The study includes tests of beams (Gribniak *et al.* 2012, Kaklauskas *et al.* 2014) and slabs (Barros *et al.* 2008) with ranging amounts of fibres and predominantly low reinforcement ratio of longitudinal bars.

Nine beams with reinforcement ratios of 0.3 and 0.6% and steel fibres contents of 0.5, 1.0 and 1.5% by volume were selected (Gribniak *et al.* 2012, Kaklauskas *et al.* 2014). The beam specimens with 0.6% reinforcement ratio are numbered S2-F05, S2-F10 and S2-F15 (taking S2-F10

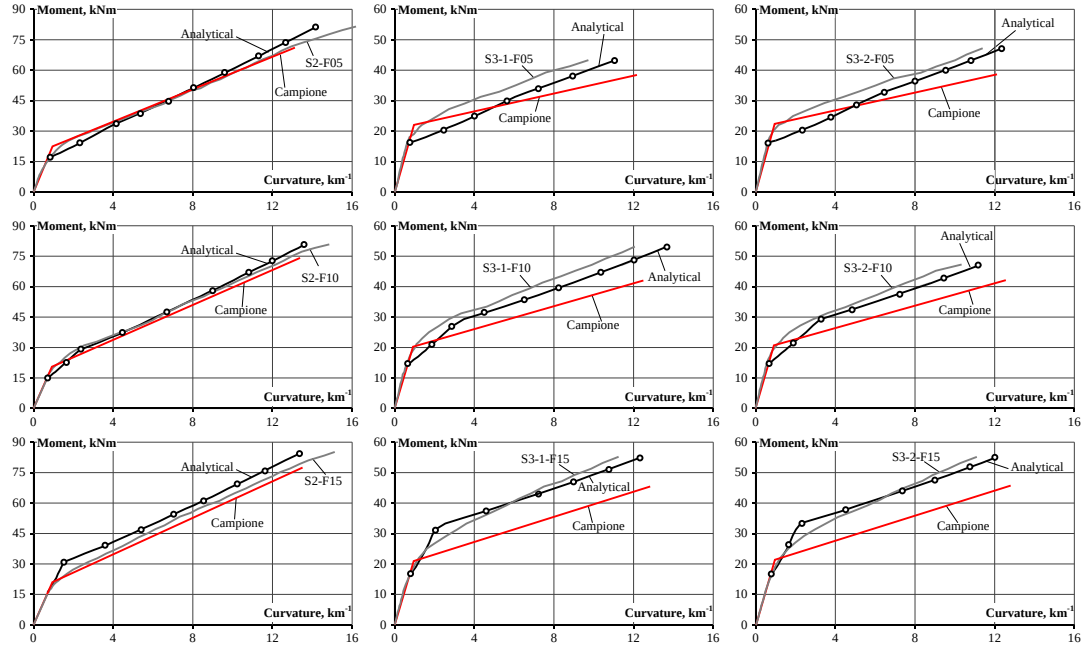

Fig. 7 Experimental and analytical moment-curvature diagrams of beams

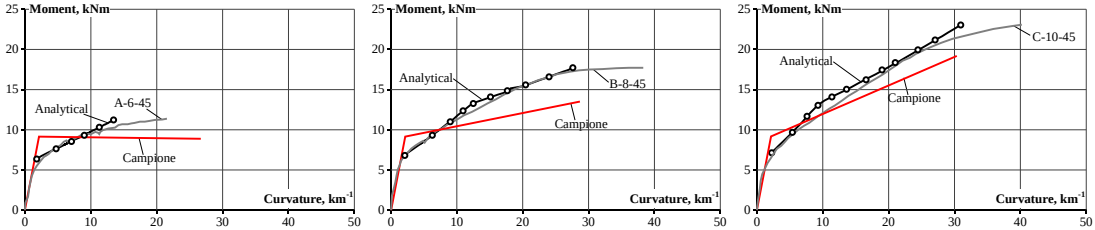

Fig. 8 Experimental and analytical moment-curvature diagrams of slabs

as an example, S2 denotes the group of specimens with 0.6% of reinforcement, and F10 means the fibre volume ratio of 1.0%). The beam specimens with 0.3% reinforcement ratio are duplicated (twin beam specimens were made and tested). In addition to the three specimens numbered S3-1-F05, S3-1-F10 and S3-1-F15, three replicated specimens with respectively the same characteristics are numbered S3-2-F05, S3-2-F10 and S3-2-F15 (taking S3-1-F10 and S3-2-F10 as an example, they are identical samples in the group of specimens with 0.3% of reinforcement, and with fibre volume ratio of 1.0%).

Table 2 lists the main parameters of the test specimens. In this table, f_{sy} and E_s are the yield stress and the elastic modulus of the bar reinforcement, respectively; f_{cm} is the average compressive strength of 150×300 mm concrete cylinder at the age of testing; V_f is the volume content of fibres in the concrete mixture. Other notations are given in Fig. 5. All the beams were of rectangular cross-section with nominal length of 3280 mm and span length of 3000 mm.

The beams were tested under symmetrical four-point bending arrangement. During the loading, the deformation of the beams over the pure bending zone was monitored using mechanical gauges arranged at four levels of gauge lines respectively along: (1) the centreline of tension reinforcement, (2) 60 mm offset above the centreline of tension reinforcement, (3) 60 mm offset below the centreline of compression reinforcement, and (4) the centreline of compression reinforcement. The curvature in the pure bending zone was evaluated from the mechanical gauge reading according to the following equation

$$\kappa = \frac{1}{6}\sum_{l=2}^{4}\sum_{k=1}^{l-1}\frac{D_k - D_l}{h_{kl}} \tag{33}$$

where D_k and D_l are respectively the averaged strains along k and l gauge lines (1st to 4th), h_{kl} is the distance between the lines (k, l=1 to 4, and $k \neq l$). All the slab strips were of rectangular cross-section with nominal length of 1600 mm and span length of 1350 mm, as shown in Fig. 6. The slabs were tested under symmetrical four-point bending arrangement. During the loading, the deflections were measured using multiple LVDTs (linear variable displacement transducers) along the span.

The main parameters of test slabs (Barros *et al.* 2008) are also listed in Table 2. It includes three slab strip specimens with reinforcement ratios of 0.2, 0.3 and 0.5% and steel fibres content of 0.6% by volume. The slab strip specimens are numbered A-6-45, B-8-45 and C-10-45 (taking A-6-45 as an example, it means that 6 mm diameter steel reinforcement was employed and the steel fibre content was 45 kg per m^3 of concrete).

Fig. 7 and Fig. 8 summarises the moment-curvature relations of R/SFRC beams and slabs, respectively, obtained

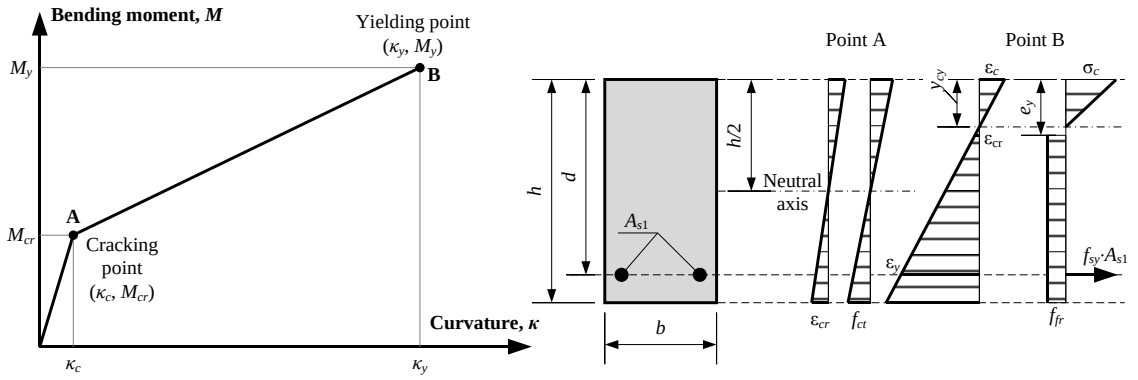

(a) (b)

Fig. 9 Simplified moment-curvature diagram proposed by Campione (2008)

by both the analytical technique and by the experimental testing. Comparing the two groups of results of beams in Fig. 7, in general good agreement between the analytical and experimental data is observed. Relatively, better predictions are obtained for group S2 specimens (with 0.6% reinforcement ratio). Among the specimens in group S2, more accurate evaluations are achieved for the cases of lower contents of steel fibres (0.5% and 1.0%). On the contrary, for group S3 specimens (with 0.3% reinforcement ratio), the computed flexural responses are generally less stiff than the experimental data. The curvature prediction errors were due to the scatter of test results and the use of simplified constitutive relations for residual strength (Eq. (17)) and tension stiffening (Eq. (27)). This error can be partly mitigated by using an alternative and more accurate tension stiffening relationship (Kaklauskas and Sokolov 2021). As regards the analytical results of slab strips as shown in Fig. 8, good agreement with experimental results is obtained.

The computational model proposed by Campione (2008) is applied to analyse the moment-curvature response of the beam and slab strip specimens. The approach illustrated in Fig. 9 is based on linear interpolation between two curvature values corresponding to the cracking moment M_{cr} and the yielding moment M_y. In the model, the tension stiffening phenomenon is not directly taken into account, and the contribution of the longitudinal compression reinforcement is neglected due to its marginal influence in contrast to the reinforcement in tension. Curvature at the serviceability limit state is determined through a two-stage process:

Stage 1. Cracking point (κ_c, M_{cr}): As suggested by Naaman (2003), the cracking resistance is assessed for the elastic section assuming tensile strength $f_{ct}=0.7(f_{cm})^{0.5}$ (where f_{cm} is the mean cylindrical compressive strength of concrete) (see Fig. 9(b)). The respective curvature is obtained from the following equation

$$\kappa_c = \frac{12\,M_{cr}}{bh^3E_c} \tag{34}$$

Stage 2. Yielding point (κ_y, M_y): As shown in Fig. 9(b), yielding stress is taken for the tensile reinforcement and the elastic behaviour is assumed for compressive concrete. Residual stress f_{fr} of the rectangular stress block is calculated per Eqs. (17) and (18). The model supposes that residual stress f_{fr} is initiated at the fibre concrete submitted to cracking strain, ε_{cr}, Fig. 9(b). Therefore, two geometrical parameters, namely y_{cy} (the depth of neutral axis at yielding) and e_y (the vertical distance between the extreme compression fibre of concrete and the point where cracking strain of the tensile concrete is reached) are needed to describe the stress and strain diagrams in the concrete zones in compression and tension (Fig. 9(b)). The parameters y_{cy} and e_y can be obtained by solving the following two equations

$$\frac{E_c f_{sy}}{2E_s}\frac{y_{cy}}{d-y_{cy}}by_{cy} - f_{sy}A_s - f_{fr}b\left(h-e_y\right) = 0 \tag{35}$$

$$e_y = \frac{\frac{2f_{ct}}{E_c}(d-y_{cy})+\varepsilon_y\,y_{cy}}{\varepsilon_y} \tag{36}$$

Upon determining the values of y_{cy} and e_y, the two required unknowns (M_y and κ_y) are found from the following equations

$$M_y = bd^2\left[\rho f_{sy}\left(1-\frac{0.33y_{cy}}{d}\right)+f_{fr}\left(\frac{h-e_y}{d}\right)\left(\frac{y_{cy}}{1.5d}-\frac{h-e_y}{2d}\right)\right] \tag{37}$$

$$\kappa_y = \frac{f_{sy}}{E_s(d-y_{cy})} \tag{38}$$

It should be noted that while the assumption of the elastic behaviour for the compressive fiber concrete seems justifiable for the case of lightly reinforced members, it may be the source of significant inaccuracies of curvature analysis for the members with large reinforcement ratio due considerable nonlinear behaviour of FRC in compression at the yield load. Another disadvantage of the technique described in (Campione 2008) is that it permits calculating curvature based on linear interpolation between the two specified points, but is not capable of predicting the stress and strain states at a given load level.

In order to visually compare the model by Campione (2008) with the proposed analytical technique and the experimental results, the computation results based on Campione (2008) are also plotted in Fig. 7 and Fig. 8. Generally, it is seen that the proposed model herein is capable of predicting more accurate results than the model by Campione (2008), particularly for the group S3 beam

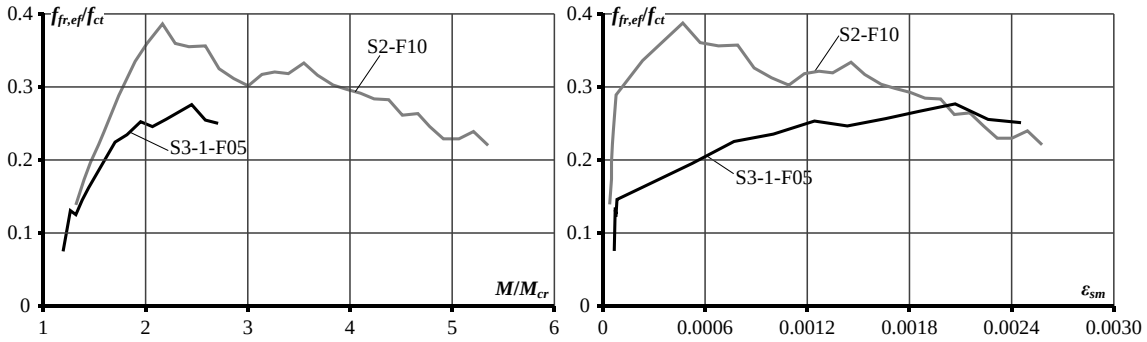

Fig. 10 Effective residual stress values of beams S2-F10 and S3-1-F05: (a) variation with bending moment; and (b) variation with mean steel strain

specimens (with low reinforcement ratio of 0.3%) and slab specimens. Among the specimens analysed, the model by Campione (2008) basically overestimates the curvature at the loads throughout the cracked regime with the exception of early stages of cracking when the predictions were too stiff. Such deviations would be mainly due to the inaccurate assessment of the combined effects of residual stress and tension stiffening (Taheri *et al.* 2012). The largest errors were obtained for group S3 beams having reinforcement ratio of 0.3% (Fig. 7).

6. Variations of effective residual stresses in SFRC members

Tension stiffening and the residual stress are two highly interrelated effects that are difficult to quantify having a significant contribution to the stiffness of R/SFRC members. In a way as demonstrated in Section 3, the residual stress can be derived from the inverse analysis by considering the curvature response of a R/SFRC member. In this context, the term of *effective* residual stress is introduced as discussed below. To assess the contribution of steel fibres to the flexural tension resistance of R/SFRC members with conventional longitudinal reinforcement, the *effective* residual stresses $f_{fr;ef}$ of the beam specimens are back-calculated from the experimental moment-curvature responses by the iterative inverse approach. The variations of residual stress with the applied bending moment and with the mean steel strain for two beam specimens, S2-F10 and S3-1-F05, are shown in Fig. 10. The *effective* residual stress is normalised with respect to the tensile strength of concrete ($f_{fr;ef}/f_{ct}$) assessed per the Model Code 2010 (2013) provisions, and the bending moment is normalised with respect to the cracking moment (M/M_{cr}). From Fig. 10a, it can be seen that the *effective* residual stress of beam S2-F10 with 1% fibre volume ascended steadily to the peak point at M/M_{cr} approximately equal to 2, and then descended gradually; while the residual stress of beam S3-1-F05 with 0.5% fibre volume increased nonlinearly to the peak point at M/M_{cr} approximately equal to 2.5, and followed by a short descending branch. The peak of normalised effective residual stress of beam S2-F10 was approximately 40% higher than that of beam S3-1-F05. Similarly, from Fig. 10b, it is also seen that the effective residual stress of beam S2-F10 reached the peak point at a smaller mean steel strain level than beam S3-1-F05, and the residual stress decreased with a substantially longer descending branch for beam S2-F10.

The depicted trends illustrate the development of *effective* residual stress during the crack formation stage of R/SFRC flexural members. The results presented in Fig. 10(a) are in support of Assumption 5 stating that residual stress varies linearly from 0 to f_{fr} proportionally to the applied bending moment ranging between M_{cr} and ζM_{cr} (see Fig. 1(b)).

As noted earlier, the tensile resistance of cracked R/SFRC members is contributed by both the tension stiffening effect and the steel fibres across cracks. Research on the cracking and tension stiffening behaviour of R/SFRC tension members containing conventional reinforcing bars had confirmed that the onset of cracking and post-crack response of SFRC were altered by the presence of conventional reinforcement (Amin *et al.* 2016, Amin *et al.* 2017, Deluce and Vecchio 2013, Tiberti *et al.* 2015). The relative contribution of each of the above effects varies with the loading level and the structural configurations, and this should be the subject of further investigations so as to establish the rate of development of effective residual stress under increasing load. By so doing, the approach can be extended to analysis of continuously supported beams subjected to intermediate loading (Dundar *et al.* 2015), thus allowing more general applications. Comparing the *effective* residual stresses across different R/SFRC beam specimens, the variation of $f_{fr;ef}$ is affected by the steel fibre contents and reinforcement ratio. Therefore, to accurately predict the flexural response of R/SFRC members, the evaluation of effective residual stress should take into account the steel fibre volumes and the reinforcement ratios. Further research for the rigorous formulation of the effective residual stress is advocated.

7. Conclusions

A new analytical technique for analysing steel fibre-reinforced concrete (SFRC) members with conventional longitudinal reinforcement (denoted as R/SFRC) under flexure has been developed. The technique is based on rational assumptions. The tension stiffening effect of

cracked concrete has been considered with the tension stiffening stress attributed to the reinforcement, and the tension stiffening force of equivalent reinforced concrete and R/SFRC members at a given strain level of tensile reinforcement in the cracked section are assumed to be equal. In the tension zone of concrete, the intensity of rectangular stress block is taken as the residual tensile stress of SFRC, which has been established based on the formulation proposed by Naaman (2003) with modifications. This circumvents the need of conducting mechanical testing for individual cases. It has been assumed that within the early stages of cracking, the residual tensile stress increases linearly from zero to f_{fr} proportionally to the bending moment ranging between M_{cr} and ζM_{cr}. The physical justification behind this assumption is that each new crack in the crack formation stage induces tension softening stresses that gradually contribute to the stiffness of the structure. When the loading exceeds ζM_{cr}, the residual stress is taken constant as f_{fr}. To progress with the analysis, stepwise calculations are performed for moment-curvature analysis. In each loading step, the curvature corresponding to the external moment is determined.

To validate the proposed analytical technique, nine SFRC beam specimens of six different configurations and three SFRC slab strip specimens with different values of reinforcement ratios and fibre volume fractions have been selected and analysed. The moment-curvature relations predicted from the proposed technique have been compared with the experimental results. Good agreement between the experimental and analytical results has been observed, and the proposed technique performed better for the group of beam specimens with 0.6% reinforcement ratio than those with 0.3% reinforcement ratio. The less desirable accuracy for specimens with low reinforcement ratio would be related to the inaccuracy of the Model Code to predict the tension stiffening of flexural members with small amount of reinforcement. Furthermore, the moment-curvature relations of the SFRC beams and slabs have been evaluated based on the computation model proposed by Campione (2008). Comparatively, the proposed technique by the authors has yielded results in closer agreement with the test data. For the group of beam specimens with lower reinforcement ratio (0.3%) and for the slab specimens, the deviations between test data and modelling results per Campione (2008) are more substantial.

The study has introduced the concept of effective residual stress which is regarded as the tensile stress in the R/SFRC that, in addition to the tension stiffening stresses, secures adequate deformation response of the given member. The effective residual stresses of the beam specimens have been back-calculated from the moment-curvature responses. It was found that the effective residual stresses increase gradually during the crack formation stage to reach the respective peak value, and the variation trends of effective residual stresses are affected by the steel fibre volume and the reinforcement ratio. Further investigations on the rate of development of effective residual stress in cracked R/SFRC members under increasing load and its dependence on the structural configurations are recommended.

Acknowledgments

This project has received funding from European Social Fund (Project No. 09.3.3-LMT-K-712-01-0145) under a grant agreement with the Research Council of Lithuania (LMTLT).

References

Abrishambaf, A., Barros, J.A.O. and Cunha, V. (2015), "Tensile stress-crack width law for steel fibre reinforced self-compacting concrete obtained from indirect (splitting) tensile tests", *Cement Concrete Compos.*, **57**, 153-165. https://doi.org/10.1016/j.cemconcomp.2014.12.010.

ACI 544.4R-88 (1988), Building Code Requirements for Structural Concrete and Commentary, American Concrete Institute, Michigan.

Alsayed, S.H. (1993), "Flexural deflection of reinforced fibrous concrete beams", *ACI Struct. J.*, **90**, 72-76.

Amin, A. and Gilbert, R.I. (2018), "Instantaneous crack width calculation for steel fiber reinforced concrete flexural members", *ACI Struct. J.*, **115**(2), 535-543.

Amin, A., Foster, S.J. and Kaufmann, W. (2017), "Instantaneous deflection calculation for steel fiber reinforced concrete one way members", *Eng. Struct.*, **131**, 438-445. http://dx.doi.org/10.1016/j.engstruct.2016.10.041.

Amin, A., Foster, S.J. and Muttoni, A. (2015), "Derivation of the σ-w relationship for SFRC from prism bending tests", *Struct. Concrete*, **16**(1), 93-105. https://doi.org/10.1002/suco.201400018.

Amin, A., Foster, S.J. and Watts, M. (2016), "Modelling the tension stiffening effect in SFR-RC", *Mag Concrete Res.*, **68**(7), 339-352. https://doi.org/10.1680/macr.15.00188.

Amin, A., Foster, S.J., Gilbert, R.I. and Kaufmann, W. (2017), "Material characterisation of macro synthetic fibre reinforced concrete", *Cement Concrete Compos.*, **84**, 124-133. https://doi.org/10.1016/j.cemconcomp.2017.08.018.

Ashour, S.A. and Wafa, F.F. (1993), "Flexural behavior of high-strength fiber reinforced concrete beams", *ACI Struct. J.*, **90**, 279-287.

ASTM C1609/C1609M-12 (2012), Standard Test Method for Flexural Performance of Fiber-Reinforced Concrete (Using Beam with Third-Point Loading), American Society for Testing and Materials.

ASTM C496-17 (2017), Standard Test Method for Splitting Tensile Strength of Cylindrical Concrete Specimens, American Society for Testing and Material.

Barros, J.A.O. and Figueiras, J. (1999), "Flexural behavior of SFRC: testing and modeling", *J. Mater. Civil Eng.*, ASCE, **11**(4), 331-339. https://doi.org/10.1061/(ASCE)0899-1561(1999)11:4(331).

Barros, J.A.O., Santos, S.P.F., Lourenço, L.A.P. and Gonçalves, D. (2008), "Flexural behaviour of steel fibre reinforced self-compacting concrete laminar structures", *Proceedings, 1st Spanish Congress on Self-Compacting Concrete*, Valencia, Spain, February.

Barros, J.A.O., Taheri, M. and Salehian, H. (2017), "A model to predict the crack width of FRC members reinforced with longitudinal bars", *ACI Spec. Publ.*, **SP-319**, 2.1-2.16.

Broberg, K.B. (1999), *Cracks and Fracture*, Elsevier.

Campione, G. (2008), "Simplified flexural response of steel fiber-reinforced concrete beams", *J. Mater. Civil Eng.*, ASCE, **20**(4), 283-293. https://doi.org/10.1061/(ASCE)0899-1561(2008)20:4(283).

Campione, G., La Mendola, L. and Papia, M. (2006), "Shear strength of fiber reinforced beams with stirrups", *Struct. Eng. Mech.*, **24(1)**, 107-136. https://doi.org/10.12989/sem.2006.24.1.107.

Chu S.H. and Kwan A.K.H. (2021), "Crack mitigation utilizing enhanced bond of rebars in SFRC", *Struct.*, **33**, 4141-4147. https://doi.org/10.1016/j.istruc.2021.06.095.

Comité Euro-International du Beton (CEB) (2013), CEB-FIP Model Code 2010: Model Code for Concrete Structures, Ernst & Sohn, Wiley, Berlin, Germany.

Craig, R.J. (1987), "Flexural behavior and design of reinforced fiber concrete members", *ACI Spec. Publ.*, **105**, 517-564.

Cunha, V.M.C.F. (2010), "Steel fibre reinforced self-compacting concrete (from micro-mechanics to composite behaviour)", Doctoral Thesis, University of Minho.

Cunha, V.M.C.F., Barros, J.A.O. and Sena-Cruz, J.M. (2010), "Pullout behaviour of steel fibres in self-compacting concrete", *J. Mater. Civil Eng.*, ASCE, **22**(1), 1-9. https://doi.org/10.1061/(ASCE)MT.1943-5533.0000001.

DAfStb (2012), Deutscher Ausschuss für Stahlbeton, Deutscher Ausschuss Für Stahlbeton, Budapester Straße 31, D-10787 Berlin.

de Montaignac, R., Massicotte, B. and Charron, J.P. (2012), "Design of SFRC structural elements: flexural behaviour prediction", *Mater. Struct.*, **45**(4), 623-636. https://doi.org/10.1617/s11527-011-9785-y.

Deluce, J.R. and Vecchio, F.J. (2013), "Cracking behavior of steel fiber reinforced concrete members containing conventional reinforcement", *ACI Struct. J.*, **110**(3), 481-490.

Domski, J. and Zakrzewski, M. (2020), "Deflection of steel fiber reinforced concrete beams based on waste sand", *Mater.*, **13**(2), 392. https://doi.org/10.3390/ma13020392.

Dundar, C., Tanrikulu, A.K. and Frosch, R.J. (2015), "Prediction of load-deflection behaviour of multi-span FRP and steel reinforced concrete beams", *Compos. Struct.*, **132**, 680-693. https://doi.org/10.1016/j.compstruct.2015.06.018.

EN 14651 (2005), Test Method for Metallic Fibered Concrete-Measuring the Flexural Tensile Strength (Limit of Proportionality (Lop), Residual), European Committee for Standardization.

Ezeldin, A.S. and Shiah, T.W. (1995), "Analytical immediate and long-term deflections of fiber-reinforced concrete beams", *J. Struct. Eng.*, **121**, 727-738. https://doi.org/10.1061/(ASCE)0733-9445(1995)121:4(727).

Gilbert, R.I. and Warner, R.F. (1978), "Tension stiffening in reinforced concrete slabs", *J. Struct. D.*, ASCE, **104**(12), 1885-1900. https://doi.org/10.1061/JSDEAG.0005054.

Gribniak, V., Kaklauskas, G., Kwan, A.K.H., Bacinskas, D. and Ulbinas, D. (2012), "Deriving stress-strain relationships for steel fibre concrete in tension from tests of beams with ordinary reinforcement", *Eng. Struct.*, **42**, 387-395. https://doi.org/10.1016/j.engstruct.2012.04.032.

Harvinder, S. (2020), "Closed-form solution for shear strength of steel fiber-reinforced concrete beams", *ACI Struct. J.*, **117**(3), 261-269.

Hsu, C.T.T., He, R.L. and Ezeldin, S. (1992), "Load-deformation behavior of steel fiber reinforced concrete beams", *ACI Struct. J.*, **89**, 650-657.

JSCE (1984), Method of Tests for Flexural Strength and Flexural Toughness of Steel Fiber Reinforced Concrete. Part III-2 Method of Tests for Steel Fiber Reinforced Concrete, SF4 - The Japan Society of Civil Engineers, **3**, 58-61.

Kaklauskas, G. (2017), "Crack model for RC members based on compatibility of stress-transfer and mean-strain approaches", *J. Struct. Eng., ASCE*, **143**(9), 04017105. https://doi.org/10.1061/(ASCE)ST.1943-541X.0001842.

Kaklauskas, G. and Ghaboussi, J. (2001), "Stress-strain relations for cracked tensile concrete from RC beam tests", *J. Struct. Eng., ASCE*, **127**(1), 64-73. https://doi.org/10.1061/(ASCE)0733-9445(2001)127:1(64).

Kaklauskas, G. and Gribniak, V. (2011), "Eliminating shrinkage effect from moment-curvature and tension-stiffening relationships of reinforced concrete members", *J. Struct. Eng., ASCE*, **137**(12), 1460-1469. https://doi.org/10.1061/(ASCE)ST.1943-541X.0000395.

Kaklauskas, G. and Gribniak, V. (2016), "Hybrid tension stiffening approach for decoupling shrinkage effect in cracked reinforced concrete members", *J. Eng. Mech., ASCE*, **142**(11), 04016085. https://doi.org/10.1061/(ASCE)EM.1943-7889.0001148.

Kaklauskas, G. and Sokolov, A. (2021), "A peculiar value of M to M_{cr} ratio: Reconsidering assumptions of curvature analysis of reinforced concrete beams", *J. Appl. Eng. Sci.*, **7**, 100053. https://doi.org/10.1016/j.apples.2021.100053.

Kaklauskas, G., Gribniak, V., Meskenas, A., Bacinskas, D., Juozapaitis, A., Sokolov, A. and Ulbinas, D. (2014), "Experimental investigation of the deformation behavior of SFRC beams with an ordinary reinforcement", *Mech. Compos. Mater.*, **50**(4), 417-426. https://doi.org/10.1007/s11029-014-9428-9.

Kaklauskas, G., Gribniak, V., Salys, D., Sokolov, A. and Meskenas, A. (2011), "Tension-stiffening model attributed to tensile reinforcement for concrete flexural members", *Procedia Eng.*, **14**, 1433-1438. https://doi.org/10.1016/j.proeng.2011.07.180.

Kaklauskas, G., Ramanauskas, R. and Jakubovskis R. (2017), "Mean crack spacing modelling for RC tension elements", *Eng. Struct.*, **150**(1), 843-851. https://doi.org/10.1016/j.engstruct.2017.07.090.

Lackner, R. and Mang, H.A. (2003), "Scale transition in steel-concrete interaction. Part I: Model", *J. Eng. Mech.*, ASCE, **129**(4), 393-402. https://doi.org/10.1061/(ASCE)0733-9399(2003)129:4(393).

Lehmann, M. and Głodkowska, W. (2021), "Shear capacity and behaviour of bending reinforced concrete beams made of steel fibre-reinforced waste sand concrete", *Mater.*, **14**(11), 2996. https://doi.org/10.3390/ma14112996.

Lim, T., Paramasivam, P. and Lee, S. (1987), "Behavior of reinforced steel-fiber-concrete beams in flexure", *J. Struct. Eng.*, **113**, 2439-2458. https://doi.org/10.1061/(ASCE)0733-9445(1987)113:12(2439).

Marti, P., Alvarez, M., Kaufmann, W. and Sigrist V. (1998), "Tension chord model for structural concrete", *Struct. Eng. Int.*, **8**(4), 287-298. https://doi.org/10.2749/101686698780488875.

Mazaheripour, H., Barros, J.A.O. and Sena-Cruz, J.M. (2016), "Tension-stiffening model for FRC reinforced by hybrid FRP and steel bars", *Compos. Part B J.*, **88**, 162-181. http://dx.doi.org/10.1016/j.compositesb.2015.10.042.

Mazaheripour, H., Barros, J.A.O., Soltanzadeh, F. and Sena-Cruz J. (2016), "Deflection and cracking behavior of SFRSCC beams reinforced with hybrid prestressed GFRP and steel reinforcements", *Eng. Struct.*, **125**, 546-565. https://doi.org/10.1016/j.engstruct.2016.07.026.

Meskenas, A., Ramanauskas, R., Sokolov, A., Bacinskas, D. and Kaklauskas, G. (2021), "Residual stress-strain relations inversely derived from experimental moment-curvature response of RC beams with fibres compared to the recommendations of design codes", *Struct.*, **34**, 3363-3375. https://doi.org/10.1016/j.istruc.2021.09.070.

Minelli, F. and Plizzari, G.A. (2015), "Derivation of a simplified stress-crack width law for fiber reinforced concrete through a revised round panel test", *Cement Concrete Compos.*, **58**, 95-104. https://doi.org/10.1016/j.cemconcomp.2015.01.005.

Naaman, A.E. (2003), "Strain hardening and deflection hardening fiber reinforced cement composites", *Proc. 4th Int. RILEM Workshop on High Performance Fiber Reinforced Cement Composites*, Ann Abor, University of Michigan, 95-113.

Neumark, S. (1965), *Solution of Cubic and Quartic Equations*, Pergamon Press, Headington Hall, Oxford.

Ng, P.L., Lam, J.Y.K. and Kwan, A.K.H. (2010), "Tension

stiffening in concrete beams. Part 1: FE analysis", *Proc. Inst. Civil Eng.: Struct. Build.*, **163**(1), 19-28. https://doi.org/10.1680/stbu.2009.163.1.19.
RILEM TC 162-TDF (2000), "Test and design methods for steel fibre reinforced concrete: Recommendations", *Mater. Struct.*, **33**, 3-5. https://doi.org/10.1007/BF02481689.
RILEM TC 162-TDF (2002), "Test and design methods for steel fibre reinforced concrete: Design of steel fibre reinforced concrete using the σ-w method: Principles and applications", *Mater. Struct.*, **35**, 262-278. https://doi.org/10.1007/BF02482132.
RILEM TC 162-TDF (2003), "Test and design methods for steel fibre reinforced concrete: σ-ε-design method: Final recommendation", *Mater. Struct.*, **36**, 560-567. https://doi.org/10.1007/BF02480834.
RILEM TC 162-TDF. (2001), "Test and design methods for steel fibre reinforced concrete: Uni-axial tension test for steel fibre reinforced concrete", *Mater. Struct.*, **34**, 3-6. https://doi.org/10.1007/BF02482193.
Shi, Z. (2009), *Crack Analysis in Structural Concrete*, Burlington, USA, Butterworth-Heinemann Elsevier.
Skocek, J. and Stang, H. (2008), "Inverse analysis of the wedge-splitting test", *Eng. Fract. Mech.*, **75**, 3173-3188. https://doi.org/10.1016/j.engfracmech.2007.12.003.
Soltanzadeh, F., Cunha, V.M.C.F. and Barros, J.A.O. (2019), "Assessment of different methods for characterization and simulation of post-cracking behavior of self-compacting fiber reinforced concrete", *Constr. Build. Mater.*, **227**, 116704. https://doi.org/10.1016/j.conbuildmat.2019.116704.
Stähli, P. (2008), "Ultra-fluid, oriented hybrid-fibre-concrete", Doctoral Thesis, Diss. ETH No. 17996, ETH Zurich.
Taheri, M., Barros, J.A.O. and Salehian, H. (2012), "Parametric study of the use of strain softening/hardening FRC for RC elements failing in bending", *J. Mater. Civil Eng.*, ASCE, **24**(3), 259-274. https://doi.org/10.1061/(ASCE)MT.1943-5533.0000373.
Tan, K.H., Paramasivam, P. and Tan, K.C. (1994), "Instantaneous and long-term deflections of steel fiber reinforced concrete beams", *ACI Struct. J.*, **91**, 384-393.
Tiberti, G., Minelli, F. and Plizzari, G.A. (2015), "Cracking behavior in reinforced concrete members with steel fibers: a comprehensive experimental study", *Cement Concrete Res.*, **68**, 24-34. https://doi.org/10.1016/j.cemconres.2014.10.011.
Torres, L., Barris, C., Kaklauskas, G. and Gribniak, V. (2015), "Modelling of tension-stiffening in bending RC elements based on equivalent stiffness of the rebar", *Struct. Eng. Mech.*, **53**(5), 997-1016. https://doi.org/10.12989/sem.2015.53.5.997.
Torres, L., Lopez-Almansa, F. and Bozzo, L.M. (2004), "Tension-stiffening model for cracked flexural concrete members", *J. Struct. Eng.*, ASCE, **130**(8), 1242-1251. https://doi.org/10.1061/(ASCE)0733-9445(2004)130:8(1242).
UNI 11039 (2003), Steel Fiber Reinforced Concrete - Part I: Definitions, Classification Specification and Conformity - Part II: Test Method for Measuring First Crack Strength and Ductility Indexes, Italian Board for Standardization.
Wu, H.Q. and Gilbert, R.I. (2009), "Modeling short-term tension stiffening in reinforced concrete prism using a continuum-based finite element model", *Eng. Struct.*, **31**(10), 2380-2391. https://doi.org/10.1016/j.engstruct.2009.05.012.
Wu, K., Chen, F., Lin, J.F., Zhao, J.X. and Zheng, H.M. (2021), "Experimental study on the interfacial bond strength and energy dissipation capacity of steel and steel fibre reinforced concrete (SSFRC) structures", *Eng. Struct.*, **235**, 112094. https://doi.org/10.1016/j.engstruct.2021.112094.

CC

Notations

The following symbols are used in this paper:

A_{s1} : the area of the tensile reinforcement
A_{s2} : the area of the compressive reinforcement
B_0 : the coefficient for the cubic equation
B_1 : the coefficient for the cubic equation
B_2 : the coefficient for the cubic equation
B_3 : the coefficient for the cubic equation
C_0 : the polynomial coefficient
C_1 : the polynomial coefficient
C_2 : the polynomial coefficient
C_3 : the polynomial coefficient
C_4 : the polynomial coefficient
D_k : the averaged strains along k gauge lines
D_l : the averaged strains along l gauge lines
E_c : the elastic modulus of compressive concrete
E_{s1} : the elastic modulus of tensile reinforcement
E_{s2} : the elastic modulus of compressive reinforcement
F : the fibre factor
I_{cr} : the moment of inertia of the fully cracked RC section
I_{el} : the moment of inertia of the uncracked RC member
N_c : the internal force acting in the compressive concrete
N_{fr} : the resultant force of residual tensile stresses
N_{s1} : the internal force acting in tension reinforcement
N_{s2} : the internal force acting in compression reinforcement
N_{ts} : the resultant tension stiffening force
M : the external bending moment
M_{cr} : the cracking moment
M_{RC} : the bending moment
M_y : the moment at yielding point
Q : the coefficient for the quartic equation
S : the coefficient for the quartic equation
V_f : volume fraction of fibres
a_{s2} : the effective depth to the compressive reinforcement
b : the width of the element
d : the effective depth to the tensile steel area
d_f : the diameter of fibres
e_y : the vertical distance between the extreme compression fibre of concrete and the point where cracking strain of the tensile concrete is reached
f_{cm} : the average compressive strength of 150×300 mm concrete cylinder at the age of testing
f_{ct} : the mean tensile strength of concrete
f_{eq2} : the equivalent flexural tensile strength
f_{eq3} : the equivalent flexural tensile strength
f_{fr} : the residual tensile stress
$f_{fr;ef}$: the effective residual stresses
$f_{fr;modified}$: the modified residual tensile stress
$f_{fr;Naaman}$: the residual stress according to Naaman (2003)
f_{R1} : the residual flexural tensile strength corresponding to $CMOD_1$
f_{R3} : the residual flexural tensile strength corresponding to $CMOD_3$
f_{Ri} : the residual flexural tensile strength parameter
f_{sy} : the yield stress of the bar reinforcement
h : the height of the element
h_{kl} : the distance between the lines

k, l : the gauge lines
l : the length of fibres
n : the modular ratio
p : the coefficient for the quartic equation
q : the coefficient for the quartic equation
y_c : the depth of neutral axis
y_{c1} : root of the quartic equation
y_{c2} : root of the quartic equation
y_{c3} : root of the quartic equation
y_{c4} : root of the quartic equation
$y_{c,RC}$: the compressive depth of the fully cracked RC section
y_{cy} : the depth of neutral axis at yielding
Δ_0 : the coefficient for the quartic equation
Δ_1 : the coefficient for the quartic equation
ΔM : the increment of bending moment
Θ : the coefficient for the cubic equation
β : a coefficient that reflects the bond characteristics of different fibre types
ε_c : the concrete strain at extreme compression fibre
ε_{s1} : the tension steel strain
ε_{s2} : the compression steel strain
ε_s^* : the reinforcement mean strain
ε_{si} : the strain in the cracked section
ε_{sm} : the mean reinforcement strain
$\varepsilon_{sm,RC}$: the mean strain in the tensile reinforcement of RC member
ζ : an interpolation coefficient
κ_c : the curvature at cracking point
κ_{cr} : the curvature of the fully cracked section
κ_{el} : the curvature of the uncracked section
κ_m : the mean curvature of the equivalent RC member corresponding to M_{RC}
κ_y : the curvature at yielding point
λ_1 : a coefficient reflecting the expected normalized fibre pull-out length calculated as the ratio of the statistically defined fibre embedment length (l/4) over the fibre length
λ_2 : the efficiency factor of fibre orientation in the cracked state
λ_3 : the group reduction factor associated with the number of fibres pulling-out per unit area (or density of fibre crossings)
ρ : the geometrical ratio of longitudinal bars
ρ_{s1} : the ratio of tensile reinforcement
ρ_{s2} : the ratio of compressive reinforcement
σ_c : the stresses in the compressive concrete
σ_{s1} : the stresses in the tensile reinforcement
σ_{s2} : the stresses in the compressive reinforcement
σ_{si} : the stress in the cracked section
σ_{sm} : the mean reinforcement stress
σ_{ts} : the fictitious tension stiffening stress
τ : the average bond stress developed in a single fibre embedded in concrete

Appendix A. Solution of quartic equation

For a general quartic equation written as Eq. (A.1) (with the condition that C_4 is non-zero), the solution process can be deduced from the Ferrari's method by back changing the variables and using the formulae for the quadratic and cubic equations (Neumark 1965)

$$C_4 y_c^4 + C_3 y_c^3 + C_2 y_c^2 + C_1 y_c + C_0 = 0 \quad \text{(A.1)}$$

The four roots of the quartic equation, denoted as y_{c1}, y_{c2}, y_{c3} and y_{c4}, can be determined from Eqs. (A.2) and (A.3) (Neumark 1965)

$$y_{c1,2} = -\frac{C_3}{4C_4} - S \pm \frac{1}{2}\sqrt{-4S^2 - 2p + \frac{q}{S}} \quad \text{(A.2)}$$

$$y_{c3,4} = -\frac{C_3}{4C_4} + S \pm \frac{1}{2}\sqrt{-4S^2 - 2p - \frac{q}{S}} \quad \text{(A.3)}$$

where p and q can be obtained from Eqs. (A.4) and (A.5), respectively

$$p = \frac{8C_4C_2 - 3C_3^2}{8C_4^2} \quad \text{(A.4)}$$

$$q = \frac{C_3^3 - 4C_4C_3C_2 + 8C_4^2C_1}{8C_4^3} \quad \text{(A.5)}$$

Also, S can be found from Eq. (A.6)

$$S = \frac{1}{2}\sqrt{-\frac{2}{3}p + \frac{1}{3C_4}\left(Q + \frac{\Delta_0}{Q}\right)} \quad \text{(A.6)}$$

where Q can be obtained from Eq. (A.7)

$$Q = \sqrt[3]{\frac{\Delta_1 + \sqrt{\Delta_1^2 - 4\Delta_0^3}}{2}} \quad \text{(A.7)}$$

in which Δ_0 and Δ_1 can be calculated per Eqs. (A.8) and (A.9), respectively

$$\Delta_0 = C_2^2 - 3C_3C_1 + 12C_4C_0 \quad \text{(A.8)}$$

Among the four roots of the quartic equation (y_{c1} to y_{c4}), two of them are imaginary numbers, one is a real positive number and the other is a real negative number. The imaginary and negative roots are to be rejected, while the remaining positive root is to be accepted as the solution of the neutral axis depth y_c.

Appendix B. Determination of neutral axis depth of equivalent RC beam

According to Kaklauskas and Gribniak (2016), Eqs. (23) and (24) can be rearranged in a cubic form as follows

$$B_3 {y_c}^3 + B_2 {y_c}^2 + B_1 y_c + B_0 = 0 \quad \text{(B.1)}$$

in which the coefficients B_0, B_1, B_2 and B_3 are in accordance with Eqs. (B.2) to (B.5), respectively (Kaklauskas and Gribniak 2016)

$$B_0 = -\kappa_m(E_{s2} - E_c)(d - a_{s2})a_{s2}A_{s2} - M \quad \text{(B.2)}$$

$$B_1 = \kappa_m(E_{s2} - E_c)(d - a_{s2})A_{s2} \quad \text{(B.3)}$$

$$B_2 = \frac{\kappa_m E_c b d}{2} \quad \text{(B.4)}$$

$$B_3 = -\frac{\kappa_m E_c b}{6} \quad \text{(B.5)}$$

where M is to be substituted with each adopted value of the applied moment M_{RC}, and κ_m is the value of curvature in the equivalent RC beam corresponding to each value of the applied moment (M_{RC}) and can be obtained according to Section 3.

The cubic equation has three roots. Applying the physical condition $0<y_c\leq h$, the negative and imaginary roots are to be rejected, and the acceptable root can be obtained from Eqs. (B.6) and (B.7) (Kaklauskas and Gribniak 2016)

$$y_c = -\frac{[2(B_2^2 - 2B_3B_1)0.5sin\Theta + B_2]}{3B_3} \quad \text{(B.6)}$$

$$\Theta = \frac{1}{3}\sin^{-1}\left[\frac{9B_3B_2B_1 - 27B_3^2B_0 - 2B_2^3}{2(B_2^2 - 2B_3B_1)^{1.5}}\right] \quad \text{(B.7)}$$